Remote sensing vegetation indices enhance understanding of the coupling of terrestrial ecosystem evapotranspiration and photosynthesis on a global scale

Bai Yun[1 *], Zhang Sha[1], Zhang Jiahua[1,2], Wang Jingwen[2,3], Yang Shanshan[2], Vincenzo Magliulo[4], Luca Vitale[4], Zhao Yanchuang[5,6]

1 Centre for Remote Sensing and Digital Earth, College of Computer Science and Technology, Qingdao University, 266071 Qingdao, China.
2 Key Laboratory of Digital Earth Science, Institute of Remote Sensing and Digital Earth, Aerospace Information Research Institute Chinese Academy of Sciences, 100094 Beijing, China.
3 EMMAH UMR 1114, INRAE, 84914 Avignon, France
4 CNR Institute for Mediterranean Agricultural and Forest Systems, Via Patacca, 85, Ercolano (Napoli), Italy
5 College of Information Science and Engineering, Henan University of Technology, 450001 Zhengzhou, PR China
6 Instituto Multidisciplinar para el Estudio del Medio "Ramón Margalef," Universidad de Alicante, 03690 San Vicente del Raspeig, Alicante, Spain.

* Corresponding author: Bai Yun, Email: baiyun@qdu.edu.cn

Key points:

- We proposed a novel remote sensing approach to coupling ecosystem evapotranspiration (ET) and photosynthesis (GPP) (RCEEP)
- RCEEP performed reliably and better than existing methods as to reproducing GPP from ET on a global scale
- Remote sensing vegetation indices used in RCEEP remarkably contribute to the more meaningful relationship between ET and GPP

Abstract

The current approaches have known limitations to understanding the coupling of terrestrial ecosystem evapotranspiration (ET) and photosynthesis (referred to as gross primary productivity, GPP). To better characterize the relationship between ET and GPP, we developped a novel remote sensing (RS)-driven approach (RCEEP) based on the underlying water use efficiency (uWUE). RCEEP partitions transpiration (*T*) from ET using a RS vegetation index (VI)-derived ratio of *T* to ET (VI-f_T) and then links *T* and GPP via RS VI-derived G_c (VI-G_c) rather than leaf-to-air vapor pressure difference. RCEEP and other two uWUE versions (VI-T or VI-G), which only incorporate VI-f_T or VI-G_c, were evaluated and compared with the original uWUE model in terms of their performances (Nash-Sutcliffe efficiency, NSE) in estimating GPP from ET over 180 flux sites covering 11 biome types over the globe. Results revealed better performances of VI-T and VI-G compared to the original uWUE, implying remarkable contributions of VI-f_T and VI-G_c to a more meaningful relationship between ET and GPP. RCEEP yielded the best performances with a reasonable mean NSE value of 0.70 (0.76) on a daily (monthly) scale and across all biome types. Further comparisons of RCEEP and approaches modified from recent studies revealed consistently better performances of RCEEP and thus, positive implications of introducing VI-f_T and VI-G_c in bridging ecosystem ET and GPP. These results are promising in view of improving or developing algorithms on coupled estimates of ecosystem ET and GPP and understanding the GPP dynamics concerning ET on a global scale.

Plain Language Summary

Evapotranspiration and photosynthesis processes of land ecosystems are mutually affected. Reasonable representations of the relationship between the two processes

are important for us to understand the way the environment changes under the background of climate change. However, existing models that represent the evapotranspiration-photosynthesis relationship have several known limitations. To better characterize the evapotranspiration-photosynthesis relationship, we developed a novel approach to bridging evapotranspiration and photosynthesis based on vegetation information remotely sensed by satellite. We found that the novel approach could present a more meaningful relationship between ecosystem evapotranspiration and photosynthesis than the existing methods over the globe. This finding reveals positive implications of introducing remotely sensed vegetation information in reasonably representing the evapotranspiration-photosynthesis relationship. Moreover, the novel approach we developed paves a way for more insightful understanding of the evapotranspiration and photosynthesis of land ecosystems and their relationship.

Keywords: Remote sensing; Vegetation indices; Evapotranspiration; Gross primary productivity; Terrestrial ecosystems; Global

1 Introduction

Terrestrial ecosystem evapotranspiration (ET) and photosynthesis (referred to as gross primary productivity, GPP) play important roles in land-atmosphere material and energy exchanges. The two processes are also closely coupled (Beer et al., 2009; Zhou et al., 2014) due to the dominating role of transpiration (*T*) in evapotranspiration (ET) (Jasechko et al., 2013; Li et

al., 2019; Stoy et al., 2019) and the combined relationship between *T* and carbon assimilation (*A*) due to the common stomatal pathway (Cowan and Farquhar, 1977; Medlyn et al., 2011) over global terrestrial biomes. Therefore, the knowledge of the quantitative correlation between ecosystem ET and GPP can provide insightful views on modeling and understanding the earth systems. However, the relationship between ET and GPP on an ecosystem level is still only partly understood (Boese et al., 2017), so that more robust and general approaches are urgently needed.

Established theories to express the quantitative relationship between *T* and *A* are available from leaf to ecosystem-level (Beer et al., 2009; Medlyn et al., 2011; Zhou et al., 2014). Representing stomatal behavior is the key to couple the water and carbon exchanges between the plant and environment as both water loss and carbon up-taking are dominated by stomata (Cowan and Farquhar, 1977; Ball et al., 1987; Collatz et al., 1991; Leuning, 1995). The long-standing theory of optimal stomatal behavior (TOSB) (Cowan and Farquhar, 1977) and the experiment of Mott and Parkhurst (1991) indicate a direct response of stomatal conductance (g_s) to leaf-to-air vapor pressure difference (*D*). Analytical stomatal conductance model of Medlyn et al. (2011) following this TOSB consistently demonstrated the response of g_s to $\sqrt{D}$ and thus the dependence of the coupling of *T* and *A* on D on a leaf-level (see also Appendix C). The importance of D in coupling ecosystem-level ET and GPP was also widely recognized (Beer et al., 2009; Zhou et al., 2014, 2015; Cheng et al., 2017). Assuming steady-state environmental conditions with a constant value of c_i/c_a allows for bridging ecosystem-level *T* and *A* (i.e., GPP) via the inherent water use efficiency (IWUE) (Beer et al., 2009), which is defined as $\mathrm{IWUE} = \mathrm{GPP} \cdot D/T = c_a(1 - c_i/c_a)/1.6$ (see also Appendix C), where c_i and c_a denotes the inner-leaf

and ambient CO_2 partial pressure, *D* is substituted by VPD, and *T* is approximated by ET. To enhance the relationship between *T* and GPP under a changing environment, Zhou et al. (2014) approximated $(1 - c_i/c_a)$ as a proportion to $\sqrt{D}$ as indicated by Lloyd and Farquhar (1994) and introduced the concept of Underlying Water Use Efficiency (uWUE) to link *T* and GPP (see also Section 2.1). uWUE can lead to a more reliable relationship between ecosystem *T* (using ET as a surrogate) and GPP than did IWUE under changing environments, i.e., $\mathrm{uWUE} \cdot T = \mathrm{GPP}/\sqrt{D}$, which is robust from hourly to yearly scales (Zhou et al., 2014, 2015).

However, the ecosystem-level relationships between ET and GPP over global terrestrial biomes are biased by the presence of the evaporation components of ET, e.g. soil evaporation (E_s), and the difficulties to access the true value of *D*. uWUE uses ET to approximate *T* (Zhou et al., 2014, 2015), an approach prone to errors, since *T* is not a constant fraction of ET (Wang et al., 2014; Wei et al., 2017; Lian et al., 2018; Stoy et al., 2019). Multiple studies revealed variable contributions of *T* or E_s to ET over global biomes (Cavanaugh et al., 2011; Gu et al., 2018; Lian et al., 2018; Perez-Priego et al., 2018; Li et al., 2019). As E_s is free from the effect of stomatal conductance (g_s) which is in turn regulated by D (Leuning, 1995; Medlyn et al., 2011), uWUE may fail to represent the relationship between ET and GPP of ecosystems with changing E_s/ET values. Since the true value of *D* is difficult to be obtained, uWUE uses VPD as an approximate (Zhou et al., 2014, 2015). However, VPD significantly deviates from *D* due to significant temperature differences between leaf (or canopy) and ambient air (Friedl, 1995; Nelson and Bugbee, 2015), under drought (Almeida, 1986; Olufayo et al., 1993), as well as under well-watered conditions (Jackson et al., 1981; Idso, 1982; Idso et al., 1982a; Idso et al., 1982b).

The above issues relevant for a successful implementation of the uWUE approach can be

addressed using remote sensing (RS) techniques. Efforts devoted to partition *T* from ET revealed a great impact of vegetation information that can be remotely sensed on the value of E_s/ET or T/ET (denoted as f_T thereafter) (Wang et al., 2014; Zhou et al., 2016; Wei et al., 2017; Gu et al., 2018; Perez-Priego et al., 2018). For example, Wang et al. (2014) and Wei et al. (2017) showed tight correlations between the value of f_T and vegetation leaf area index (LAI). On the other end, the problem connected with a proper assessment of *D* was rarely focused (Drake et al., 2017; Li et al., 2019), due to the difficulty to acquire accurate canopy temperature or transpiration information over broad regions or long terms. Li et al. (2019) and Drake et al. (2017) used VPD_l instead of VPD to approximate *D*; however, it should be noted that VPD_l is also affected by soil evaporation. In the uWUE approach, *D* was harnessed for representing the stomatal effects on the photosynthesis-transpiration relationship. On the other hand, using g_s rather than *D* to couple ET and GPP could be more straightforward, while canopy level g_s (canopy conductance, dented as G_c) can be reasonably characterized by RS vegetation indices (VIs) (Yebra et al., 2013; Bai et al., 2017).

uWUE presents a concise and effective approach to coupling ecosystem ET and GPP but its effectiveness is limited by the sensible differences between ET and *T*, and VPD and *D*. The two issues can be potentially addressed by application of RS VIs. We exploited RS-driven approaches to coupling ecosystem ET and GPP with three main objectives:

(1) Modify the uWUE approach by linking *T* and GPP via G_c rather than *D*;

(2) Propose a novel RS-driven approach to coupling ecosystem ET and GPP based on the modified uWUE as mentioned in (1) by characterizing f_T and G_c using RS VIs;

(3) Compare the performances between the RS-driven approach, two uWUE-derived

versions which only use RS-retrieved f_T or G_c, and the original version of uWUE, concerning reproducing daily and monthly-scale GPP from ET over 180 flux sites covering multiple biome types over the globe.

(4) Furtherly explore the differences in performance between the novel RS-driven approach and other methods modified from recent studies, which aimed to reasonably partition *T* from ET or link ET and GPP on an ecosystem level, concerning estimating GPP from ET on a daily scale and over the flux sites used in (3).

2 Materials and Methods

2.1 An overview of the underlying water use efficiency

The underlying water use efficiency (uWUE) proposed by Zhou et al. (2014) provides an easy approach to coupling ecosystem-level *T* and *A* and is robust from hourly to yearly scales (Zhou et al., 2015). The uWUE is derived from Inherent Water Use Efficiency (IWUE) (Beer et al., 2009), which incorporates *D* to link *A* and *T* under the steady-state condition with a constant c_i/c_a value. Zhou et al. (2014) developed uWUE by integrating the expressions of *A* and *T* following the Fick's law (Beer et al., 2009; Nobel, 2009) and assuming c_i/c_a, to be proportional to $\sqrt{D}$ (Lloyd and Farquhar, 1994), on the basis of the theory of optimal stomatal behavior (TOSB) (Cowan and Farquhar, 1977). The following equation represents the relationship between *T* and *A* through uWUE.

$$w \cdot T = A \cdot \sqrt{D}, \quad (1)$$

where *w* denotes the underlying water use efficiency (uWUE: μmol C $(mol\ H_2O)^{-1}\ kPa^{0.5}$), which is supposed to remain constant for a specific biome (Zhou et al., 2014); *T* is the

158 transpiration measured in mol m^{-2} s^{-1}; and *D* represents the leaf-to-air vapor pressure deficit
159 measured in kPa.
160 At the ecosystem level, Eq.(1) can be expressed as the following equation:
161 $$w \cdot T = \mathrm{GPP} \cdot \sqrt{D}\,, \quad (2)$$
162 where *T* is approximated by ET in Zhou et al. (2014). *D* is not an easily acquired factor on a
163 regional scale, therefore Zhou et al. (2014) and Zhou et al. (2015) used VPD to approximate *D*,
164 assuming leaf temperature is the same as air temperature, a hypothesis widely accepted (Medlyn
165 et al., 2011; Zhang et al., 2016; Boese et al., 2017; Medlyn et al., 2017). However, VPD may fail
166 to properly approximate *D*, as considerable differences in temperature between leaf and air are
167 commonly found (Jackson et al., 1981; Idso et al., 1982b; Almeida, 1986; Olufayo et al., 1993;
168 Nelson and Bugbee, 2015), which may induce substantial uncertainties in representing the
169 transpiration-photosynthesis relationship.

170 2.2 Remote sensing-driven approach to Coupling Ecosystem Evapotranspiration and
171 Photosynthesis (RCEEP)

172 2.2.1 Linking ecosystem ET and GPP via canopy conductance

173 Stomata is the main pathway for water loss and carbon uptake of plant leaves (Cowan and
174 Farquhar, 1977; Beer et al., 2009; Medlyn et al., 2011), and *D* (Eq.(2)) in the uWUE approach is
175 harnessed for representing the effect of stomatal conductance on the transpiration-photosynthesis
176 relationship. Therefore, a more straightforward approach to coupling ET and GPP is to represent
177 their relationship in terms of the g_s (G_c on a canopy or ecosystem level). G_c and *D* are linked
178 by the following relationship, according to Fick's law (Beer et al., 2009; Nobel, 2009):

$$T = \frac{D \cdot G_c}{P_a}, \quad (3)$$

where G_c is measured in mol m^{-2} s^{-1}; P_a is the atmosphere pressure (kPa). We can integrate Eq.(2) with (3) to eliminate *D* and derive the following equations to represent the relationship between ET and GPP in terms of G_c.

$$\mathrm{GPP} = w \cdot \sqrt{\frac{T \cdot G_c}{P_a}}, \quad (4)$$

$$T = f_T \cdot \mathrm{ET}, \quad (5)$$

where f_T denotes the proportion of vegetation transpiration, *T*, in ET.

2.2.2 Representing G_c and f_T using RS VIs

2.2.2.1 G_c in terms of EVI

Satellite-retrieved near-infrared vegetation indices are capable of characterizing the seasonal variations in G_c. (Zhang et al., 2009; Yebra et al., 2013; Bai et al., 2018). In this study, we incorporate a simple relationship between G_c and satellite-retrieved enhanced vegetation index (EVI).

$$G_c = k_G \cdot \mathrm{sEVI}, \quad (6)$$

$$\mathrm{sEVI} = \max\left(\mathrm{EVI} - \mathrm{EVI}_{soil}, 0\right) \cdot \left(1 - p\right) + p, \quad (7)$$

where k_G is a multiplier scaling sEVI to G_c; sEVI denotes the scaled EVI value; EVI_{soil} denotes the EVI value of soil; *p* denotes the minimum value of sEVI and is fixed to 0.01 in this study. While Yebra et al. (2013) proposed a nonlinear correlation, we propose a linear relationship between EVI and G_c, because we found EVI could linearly correlate to $\mathrm{GPP}/\left(C_a \cdot \sqrt{\mathrm{VPD}}\right)$, which is scaled with G_c, as indicated by Medlyn et al. (2011). We linearly fitted $\mathrm{GPP}/\left(C_a \cdot \sqrt{\mathrm{VPD}}\right) = \mathrm{slope} \times \mathrm{sEVI}$ to derive EVI_{soil} using the least-square method

along with daily tower-derived GPP of 180 flux sites (see also Section 2.4.1), and the value of EVI_{soil} turned out to be 0.10 ($R^2 = 0.47$).

Canopy conductance, G_c, is also regulated by many environmental parameters, e.g. air temperature, solar radiation, and leaf water potential, in addition to EVI, and thus may be more reasonably estimated by a more complicated formulation of G_c, in which these factors were accounted for. Here, we considered such a formulation, $G_c = k \cdot (sEVI \cdot \phi)^b$ (see also Text S1), where k and b are empirical coefficients and ϕ denotes the surface wetness, calculated as the ratio of actual ET to Priestley-Taylor equation derived ET potential (Priestley and Taylor, 1972). Previous studies have found ϕ tightly and nonlinearly correlated to surface conductance (Baldocchi and Xu, 2007; Ryu et al., 2008; Ma et al., 2015). Therefore, ϕ can effectively represent the environmental constraints on G_c, and the term $k \cdot (sEVI \cdot \phi)^b$ could be a better approximation for G_c than $k_G \cdot sEVI$. However, we found that such a G_c formulation showed no tendencies to facilitate a more meaningful relationship between ET and GPP (see also Section 4.2 and Text S1), as compared with that simply estimated using Eq.(6).

2.2.2.2 f_T in terms of NDVI

Ecosystem ET is by definition different from T as the contribution of soil evaporation is in most cases significant (Cavanaugh et al., 2011; Gu et al., 2018; Perez-Priego et al., 2018; Li et al., 2019). T could be partitioned from ET based on Eq. (5), where f_T is unknown. Efforts have been devoted to estimate f_T and indicated the potential of resolving this issue using remote sensing techniques (Cavanaugh et al., 2011; Zhou et al., 2016; Gu et al., 2018; Perez-Priego et al., 2018; Li et al., 2019). In this study, we evaluate a simple RS approach to approximating f_T. As ET is

primarily forced by solar radiation (Wang et al., 2010; Boese et al., 2017), we assume f_T is proportional to the Fraction of Absorbed Photosynthetically Active Radiation (f_{PAR}) (Sims et al., 2005) and estimate the former as follows:

$$f_T = k_T \cdot f_{PAR} = k_T \cdot (1.24 \times \mathrm{NDVI} - 0.168), \quad (8)$$

where k_T denotes the ratio of f_T to f_{PAR} (dimensionless). A similar approximation was made by Cheng et al. (2017), who also used f_{PAR} to approximate f_T but calculated f_{PAR} in terms of Beer's Law along with RS-derived LAI. However, due to large uncertainties existing in nowadays' LAI products (Yang et al., 2007; Jin et al., 2017), we used NDVI instead of LAI to compute f_{PAR}. We symbolized f_T computed according to Eq. (8) as NDVI-f_T.

2.2.3 RS-driven coupling of ET and GPP

Integrating Eq.(4) with Eq.(6) and (8), we can derive an original formulation linking ecosystem ET and GPP we termed 'Remote sensing-driven approach to Coupling Ecosystem Evapotranspiration and Photosynthesis' (RCEEP), representing a novel remote sensing-driven approach to coupling these two fluxes. We then compare the performances of RCEEP with the original version of the uWUE (Table 1), which uses ET and VPD to approximate *T* and *D*, respectively, for calculating GPP from ET. For better clarifying how RS VIs could facilitate more meaningful relationships between ET and GPP, we also evaluate two additional versions of RS-based approaches modified from the uWUE. The first one, formulated following Eq.(2) (VI-T in Table 1), incorporates the NDVI-derived f_T to calculate *T* from ET (Eq.(5) and (8)) and approximates *D* by VPD. The second one, formulated following Eq. (4) (VI-G in Table 1), only incorporates EVI-G_c (Eq. (6)) and approximate *T* by ET. If the use of either NDVI-f_T or EVI-G_c

plays a positive role in improving the coupling of ecosystem ET and GPP, then VI-T, VI-G, and RCEEP should all perform better than the uWUE, and RCEEP is supposed to perform the best.

Table 1 Analytical expression of uWUE, VI-T, VI-G, and RCEEP models.[a]

Model Name	RS-derived factors considered	Formulation
uWUE	-	$\mathrm{GPP} = w \cdot \mathrm{ET} / \sqrt{\mathrm{VPD}}$
VI-T	NDVI-f_T	$\mathrm{GPP} = (w \cdot k_T) \cdot (f_{PAR} \cdot \mathrm{ET}) / \sqrt{\mathrm{VPD}}$,
VI-G	EVI-G_c	$\mathrm{GPP} = \left(w \cdot \sqrt{k_G}\right) \cdot \sqrt{\mathrm{sEVI} \cdot \mathrm{ET} \cdot P_a^{-1}}$
RCEEP	NDVI-f_T and EVI-G_c	$\mathrm{GPP} = \left(w \cdot \sqrt{k_G \cdot k_T}\right) \cdot \sqrt{\mathrm{sEVI} \cdot f_{PAR} \cdot \mathrm{ET} \cdot P_a^{-1}}$

2.3 Models' Calibration and Evaluation

Undetermined constants need to be estimated in order to numerically define the relationships linking GPP and ET according to the models presented in Table 1. These coefficients are determined by fitting each model (or equation) using the least-square method and on the basis of observed flux-derived (referred to as 'observed') daily-scale GPP (GPP_{obs}) and ET (λE_{obs}) of the flux sites described in 2.4. To avoid the confounding effect of evaporation of rainfall intercepted by the canopy, we only use data from rain-free days. Data records with $GPP_{obs} \leq 1$ μmol $m^{-2}s^{-1}$ were also removed. Each value of $w \cdot k_T$, $w \cdot \sqrt{k_G}$, and $w \cdot \sqrt{k_G \cdot k_T}$ in VI-T, VI-G, and RCEEP is treated as a single quantity. Coefficients for each model were determined by directly fitting corresponding equations and are reported in Appendix A.

The four approaches presented in Table 1 are evaluated by comparing GPP estimated (GPP_{est}) using these models, along with λE_{obs} and other required inputs, against the observed GPP (GPP_{obs}) of flux sites on a daily and monthly scale. Monthly GPP_{est} is not the simple average of daily estimates but was rather estimated using the fitted equations with required

inputs. We use data of both rainy and rain-free days for the validations. We use the Nash-Sutcliffe efficiency, NSE, (Nash and Sutcliffe, 1970; Krause et al., 2005) to measure the performances of each model (Table 1), calculated as follows:

$$\mathrm{NSE} = \frac{\sum_{i=1}^{N}\left(p_i - o_i\right)^2}{\sum_{i=1}^{N}\left(o_i - \bar{o}\right)^2}, \tag{9}$$

where o_i and p_i denote observed and model-predicted values, $\bar{o}$ the average of observed values and N represents the total number of samples. The value of the index ranges from -∞ to 1 (perfect fit). Large and positive NSE values relate to good performances of the model, while values lower than zero indicates that the mean of the observations would have been a better estimate than the value predicted by the model.

The comparisons between the four models presented in Table 1 are carried out to demonstrate the importance of NDVI-f_{T} and EVI-G_{c} in the RCEEP. However, considering the recent efforts to partitioning T from ET or representing more meaningful relationships between ET and GPP on an ecosystem level, it is worthwhile to clarify the differences in performances between RCEEP and approaches modified from recent studies. Therefore, we compare RCEEP with three additional approaches modified from recent works that aimed to reasonably partition T from ET or link ET and GPP on an ecosystem level. We considered three approaches modified from recent studies, (1) RCEEP incorporating f_{T} derived from the Priestley-Taylor Jet Propulsion Laboratory (PT-JPL) (Fisher et al., 2008; Gu et al., 2018) (RCEEP-JPL), (2) WUE and ET-based carbon uptake model (WEC) (Cheng et al., 2017), and (3) uWUE incorporating solar radiation (R_{g}) (uWUE-Rg) (Boese et al., 2017). Details of the three approaches can be found in Appendix D. Both RCEEP-JPL and WEC are optimized and compared with RCEEP for

each biome types on a daily scale; while we optimize and run RCEEP and uWUE-Rg for each site on a daily scale, and the comparison between the two models is carried out on a biome level in terms of the values of their performance metric (i.e., NSE) aggregated from site-scale measurements. WEC considers canopy interception evaporation (E_i), however, modeling this ET component is beyond the scope of this study. For a fair comparison between RCEEP, RCEEP-JPL, and WEC, we used only rain-free days' data. As uWUE-Rg is designed for only rain-free days (Boese et al., 2017), we also remove data of rainy days in the comparison between RCEEP and uWUE-Rg.

2.4 Data and data processing

2.4.1 Flux site data

Site-scale observations of GPP, ET (derived from latent heat flux, λE) and required meteorological data in this study were retrieved from the FLUXNET2015 Tier 2 data (available at https://fluxnet.fluxdata.org/). This dataset provides hourly (or half-hourly), daily, weekly, monthly, and yearly water, carbon and energy fluxes as well as meteorological data. All network sites assess turbulent fluxes by means of the eddy covariance, a method that is often prone to energy imbalance issues, i.e., the sum of the observed latent heat flux and sensible heat flux is different from the available energy. We removed sites with an energy balance closure ratio (R_a) values that were smaller than 0.60 or greater than 1.30. The R_a is calculated as the following.

$$R_a = \frac{\lambda E + H}{R_n - G}$$

where H, R_n, and G denote the site level sensible heat flux, surface net radiation, and soil heat flux respectively, all measured in W m^{-2}. In addition, a site affected by prolonged snow cover

was also removed. Finally, we preserved 180 flux sites (Figure 1; see also supporting information in Table S1), which cover 13 different biome types and represent a wide range of climate conditions.

Although FLUXNET2015 dataset also provides λE and H corrected for energy balance enclosure by partitioning the residual energy between the two main dissipative heat fluxes on the basis of the Bowen ratio (Twine et al., 2000), we used the original observations, since this approach may fail in the case of short eddy covariance towers, that primarily sample small eddies. Over a heterogeneous landscape, Bowen ratios of small eddies are different from those of large eddies, which makes the energy balance closure correction factor hardly applicable (Foken, 2008). For GPP, we used the variable termed "GPP_NT_VUT_REF", where NT indicates the nighttime data-based method (Reichstein et al., 2005; Lasslop et al., 2010), VUT denotes the varied friction velocity ($u*$) threshold for filtering NEE data, and REF denotes the reference NEE value, which is the value most similar to the other 39 ones out of 40 NEE estimates. For more information concerning the derivation of GPP in FLUXNET2015 dataset, please refer to http://fluxnet.fluxdata.org/data/fluxnet2015-dataset/data-processing/.

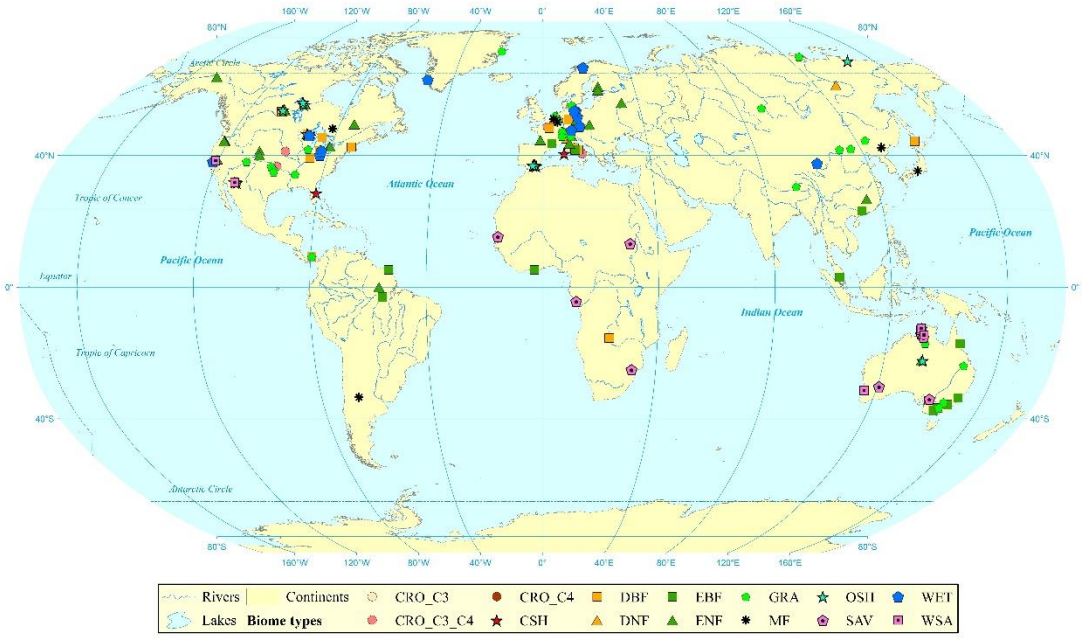

Figure 1 Distribution of the 180 flux stations used for this study over the globe (some sites appear overlapped). These sites are categorized into 13 groups in terms of biome types: CRO_C3 = C3 crops; CRO_C4 = C4 crops; CSH = close shrub; DBF = deciduous broadleaf forest; DNF = deciduous needleleaf forest; EBF = every green broadleaf forest; ENF = evergreen needleleaf forest; GRA = grassland; MF = mixed forest; OSH = open shrub; SAV = savannah; WET = wetland; and WSA = woody savannah. Frequency of each biome is as follows: CRO_C3: 8, CRO_C3_C4: 8, CRO_C4: 2, CSH: 2, DBF: 21, DNF: 1, EBF: 14, ENF: 41, GRA: 34, MF: 8, OSH: 12, SAV: 8, WET: 15 and WSA: 6. 'CRO_C3_C4' denotes a crop site where both C3 and C4 crops were grown for at least one growing season. The Projection and Geographic Coordinate Systems of this map are 'World Robinson' and 'WGS-84' and the central meridian is 0°.

We used daily data to calibrate and evaluate all models (see also section 2.3). Daily λE and GPP in the FLUXNET2015 dataset were the averages of hourly (or half-hourly, both hourly and half-hourly are referred to as hourly thereafter) values. However, if a large proportion of hourly values were unavailable, the daily value would be unreliable. For this reason, we removed daily λE or GPP data including more than 50% missing hourly values.

2.4.2 Remote sensing vegetation indices

Two vegetation indices, NDVI and EVI, were computed using the MODIS reflectance

bands.

$$\mathrm{NDVI} = \frac{\rho_{\mathrm{NIR}} - \rho_{\mathrm{RED}}}{\rho_{\mathrm{NIR}} + \rho_{\mathrm{RED}}} \quad , \tag{10}$$

$$\mathrm{EVI} = 2.5\frac{\rho_{\mathrm{NIR}} - \rho_{\mathrm{RED}}}{\rho_{\mathrm{NIR}} + 6.0\rho_{\mathrm{RED}} - 7.5\rho_{\mathrm{BLUE}} + 1} \quad , \tag{11}$$

where ρ_{NIR}, ρ_{RED}, and ρ_{BLUE} denote the reflectance of near-infrared, red, and blue bands, respectively, which were retrieved from the MOD09A1 product that has a temporal resolution of 8 days and spatial resolution of 500 m. We used the 'Global Subsets Tool', available on the website of Oak Ridge National Laboratory (https://modis.ornl.gov/data.html), to retrieve the reflectance data for each location from the pixel where the site is located. We removed low-quality pixels (surface covered by snow or cloud) at each site and calculated NDVI and EVI from the remaining data. The quality-controlled 8-day NDVI or EVI was then linearly interpolated into daily values, using the nearest available data in the time sequence.

3 Results

3.1 Cross-biome evaluation and analyses of RCEEP

Cross-validations were carried out to compare the performances of the uWUE, VI-T, VI-G, and RCEEP (Figure 2), parameterized with biome-specific factors (Appendix A) across all biomes (Figure 1) on a daily and monthly scale. The three RS-based approaches, VI-T, VI-G, and RCEEP, proved more efficient in reproducing daily and monthly GPP, featuring higher NSE values compared to uWUE, in which T and D are approximated by ET and VPD, respectively (Figure 3). On a daily scale, VI-T (NSE=0.52) and VI-G (NSE=0.71) featured better performances than the original version of uWUE (NSE=0.44), which uses no VI-derived factors, while RCEEP (using both NDVI-f_{T} and EVI-G_{c}) showed the best performance, with an NSE

value of 0.73. On a monthly scale, each model exhibited improved performance, while rankings in terms of NSE values were consistent, i.e., RCEEP > VI-G > VI-T > uWUE. Results provide evidence that incorporating both NDVI-f_T and EVI-G_c in the model can significantly contribute to improving the derivation of GPP on the basis of ET, at both daily and monthly scale.

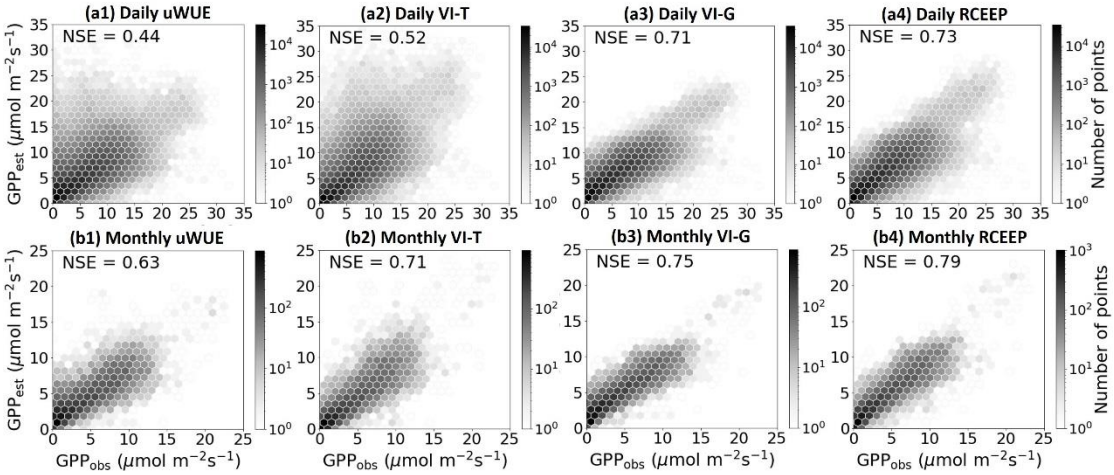

Figure 2 Comparison of Gross Primary Production estimated (GPP_{est}) by four models (uWUE, VI-T, VI-G, and RCEEP) with GPP observed at the FLUXNET ecosystem sites (GPP_{obs}) on a daily ((a1) – (a4)) and monthly ((b1) – (b4)) scale.

3.2 Biome-level evaluation and analyses of RCEEP

For each biome type, we again evaluated uWUE, VI-T, VI-G, and RCEEP (see also Table 1) parameterized with biome-specific parameters (Appendix A) with regard to reproducing GPP from ET on a daily and monthly scale (Figure 3 and Appendix B). Also, in this case, all four models featured better behavior at the monthly scale (Appendix B), since average monthly NSE values of the uWUE, VI-T, VI-G, and RCEEP were greater than daily values across all biome types, with the exception of CRO_C3 and C4 for VI-G, and RCEEP. Results highlight an inconsistent effect of incorporating NDVI-f_T and EVI-G_c on coupling ET and GPP over different biomes. VI-T and VI-G performed better than uWUE for most biome types (Figure 3)

and RCEEP was the best across all biomes except for EBF and SAV at both the daily and monthly scale (Appendix B). However, NDVI apparently failed to reflect the seasonal variations in f_T of EBF, since the inclusion of NDVI-f_T degraded the performances of both VI-T and RCEEP, while VI-G performed the best. On the other hand, VI-T and VI-G showed respectively worse and better performances than uWUE, in relation to SAV and WSA, while RCEEP performed similarly or better than VI-G (Figure 3 and Appendix B). Therefore, the inclusion of the sole NDVI-f_T act negatively on coupling ET and GPP as compared to uWUE, but it needs to be implemented along with EVI-G_c. As a whole, RCEEP can perform better than uWUE, VI-T, and VI-G over most biome types and reasonably calculate GPP from ET across all biome types with mean NSE values of 0.70 and 0.76 on a daily and monthly scale.

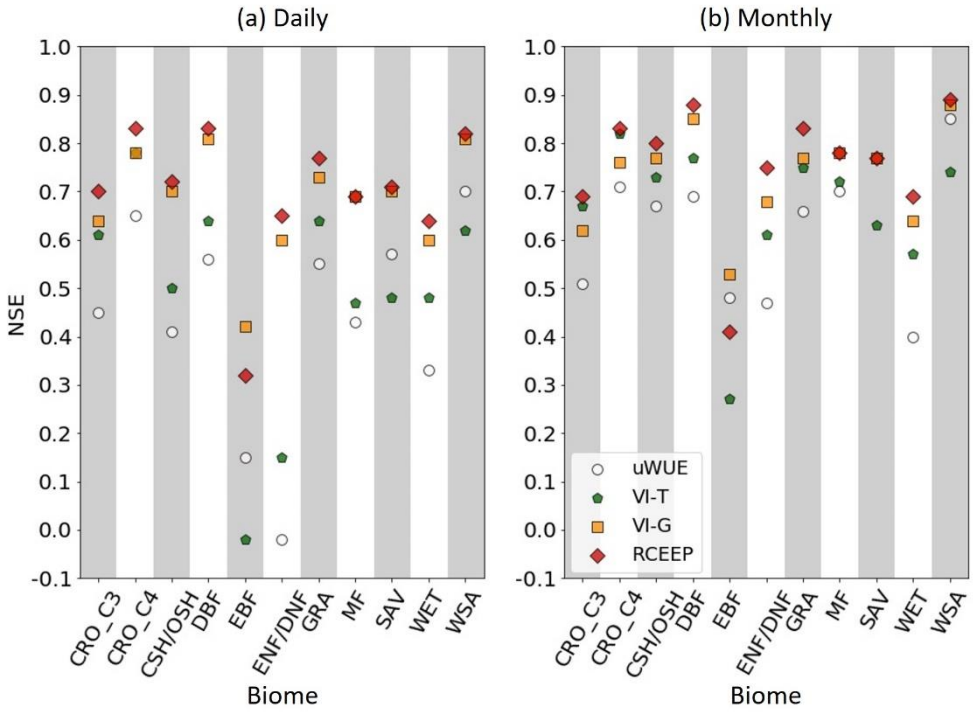

Figure 3 NSE values for validating GPP_{est} by four models (uWUE, VI-T, VI-G, and RCEEP) against GPP_{obs} over 11 biome types on a daily (a) and monthly (b) scale. Here, we refer CSH/OSH or ENF/DNF as a unique biome type, because a single DNF and two CSH sites only were present in the dataset. Abbreviations of biome type are as in Figure 1.

3.3 Comparing RCEEP with RCEEP-JPL, WEC, and uWUE-Rg

The performances of RCEEP, RCEEP-JPL, and WEC parameterized with biome-specific factors are shown in Figure 4 for each biome type, while Figure 5 presents biome-level comparisons between RCEEP and uWUE-Rg. Both Figure 4 and Figure 5 revealed better performances of RCEEP to reproduce GPP from ET on a daily scale for each biome type, on the basis of significantly greater NSE values, compared with other approaches under investigation. The biome level NSE values of RCEEP, RCEEP-JPL, and WEC are 0.71 ($\pm$0.14), 0.67 ($\pm$0.13), and 0.55 ($\pm$0.19), respectively, where values in parentheses are $\pm$1 standard deviation of NSE across all biome types. These results indicated that NDVI-f_T provided more effective estimates of the 'real' f_T than did the PT-JPL model. Although WEC used NDVI-f_T, it performed worse than both RCEEP and RCEEP-JPL. This highlights the importance of a more reasonable representation of stomatal effects in the relationship between ecosystem ET and GPP. Due to the inclusion of the site-specific parameter, *r*, in WUE-Rg, we implemented WUE-Rg and RCEEP with site-specific parameters at each flux site for a fair comparison between the two models. The results of uWUE were also included in Figure 5 as a benchmark. The results showed that while both uWUE-Rg and RCEEP can perform better than the uWUE, the latter yielded the best performances across all biome types under investigation with larger mean values of NSE.

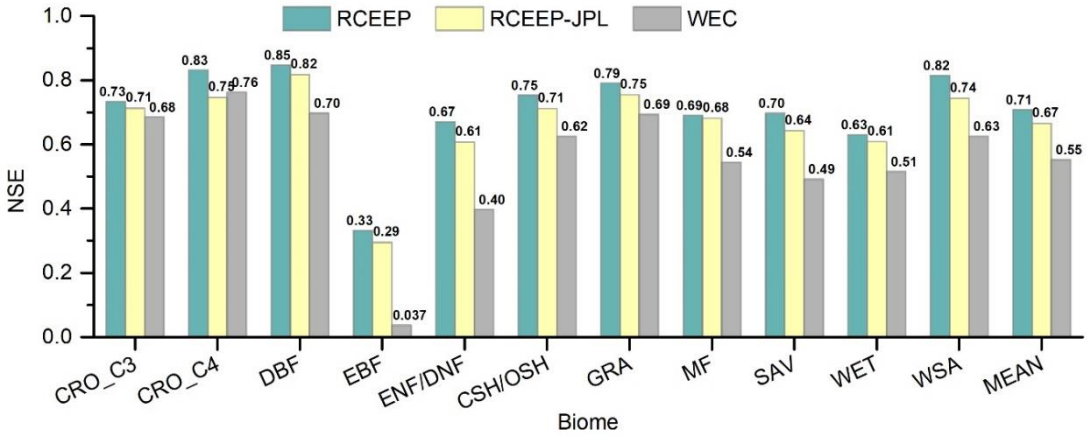

Figure 4 NSE values for RCEEP, RCEEP-JPL, and WEC with regard to reproducing GPP from ET over 11 biome types on a daily scale. 'MEAN' denotes the NSE values averaged across all biome types. Details of RCEEP-JPL and WEC can be found in Appendix D. All models are parameterized with biome-specified parameters. Refer to Figure 1 for the explanation of each biome type.

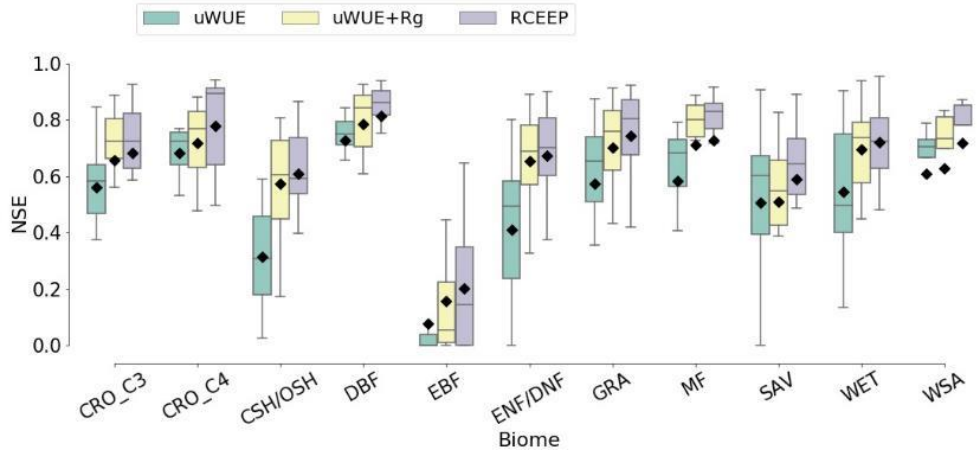

Figure 5 Distributions of the site-level NSE values of three models (uWUE, uWUE-Rg, and RCEEP) to reproducing GPP from ET based on site-specific parameters on a daily scale. Negative NSE values were forced to be 0. The details of uWUE-Rg are presented in Appendix D. Data are retrieved from rain-free days' of 160 sites with more than 300 observations. Four cropland sites (FR-Gri, IT-BCi, US-Ne2, and US-Ne3) shares CRO_C4 and CRO_C3 biomes. Refer to Figure 1 for the explanation of the biome types.

4 Discussion

4.1 VI-derived f_T

Assuming a constant f_T when building the relationships between ecosystem ET and GPP is

challenged by the variability of this parameter in relation to vegetation dynamics (Wang et al., 2014; Zhou et al., 2016; Wei et al., 2017; Perez-Priego et al., 2018). We addressed this issue by appraising f_T using NDVI-derived f_{PAR} and found that this approximation provides more effective estimates than the complex ecophysiological ET model (Figure 4), PT-JPL, which is driven by RS VIs and meteorological factors (Fisher et al., 2008). NDVI-f_T facilitated a better relationship between ecosystem ET and GPP across all biome types except for EBF. However, the usefulness of NDVI-f_T was impaired by the relatively high LAI value of dense canopies of EBF, which is generally found in tropical and subtropical regions. Satellite-retrieved NDVI is affected by canopy structure as well as by leaf chlorophyll content (Chl) (Wu et al., 2009; Croft et al., 2017), thus NDVI of a thick canopy is dominated by Chl and may fail to represent the variations in f_T.

We also found that NDVI-f_T seemed to act negatively on coupling ET and GPP of SAV and WSA, since VI-T, which uses NDVI-f_T and approximates D by VPD, yielded smaller NSE values than uWUE in reproducing GPP. On the other hand, NDVI-f_T always played a positive role when used in combination with EVI-G_c (Figure 3). To find the reason for this interesting result for SAV and WSA, we investigated the distributions of the errors in GPP_{est} from uWUE at high and low VPD values over the two biome types (Figure 6), and found uWUE tended to yield negative errors at low VPD and positive errors at high VPD values. Therefore, VPD could be a driving force of the errors in uWUE. The leaf-to-air temperature difference can fall below zero and show a negative correlation with VPD under unstressed conditions (Almeida, 1986; Olufayo et al., 1993; Nelson and Bugbee, 2015), while savannah trees show comparable well-watered conditions across both wet and dry seasons, due to their ability to access water

from deep soil layers (Herrera et al., 2012). Therefore, we speculate that the high VPD values, which generally appear in the dry season (Figure 6 (c)), could overestimate the actual value of D of SAV or WSA, and then degraded the performances of VI-T. For these biomes, high VPD values are also accompanied by low NDVI (Figure 6 (b)), which can amplify the errors induced by VPD in VI-T and thus result in worse performances. However, our study demonstrates the importance of including f_T in the model, as we found NDVI-f_T combined with EVI-G_c can lead to better performances of RCEEP compared with VI-G (see also Section 3.1 and 3.2). Perez-Priego et al. (2018) also supported our findings, who revealed significant seasonal variations in f_T, but its value rarely exceeded 80%, even in the case of a Mediterranean savannah ecosystem.

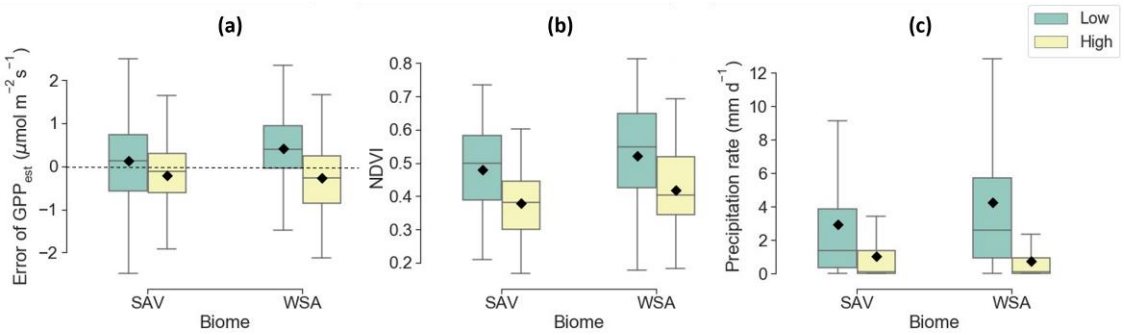

Figure 6 Distributions of (a) errors of GPP_{est} from uWUE, (b) NDVI, and (c) precipitation rate on a monthly scale for high (green boxes) and low (yellow boxes) VPD values over two biomes (SAV and WSA). The solid black diamonds represent the mean values. Kolmogorov-Smirnov tests yielded significant differences in the distributions of each variable (errors of GPP_{est}, NDVI, and precipitation rate) between low and high-VPD values over each biome. The p-value of each test is smaller than 0.001. High and Low VPD values are divided by the 50^{th} percentile of monthly VPD values in each site-year.

4.2 VI-derived G_c

The above discussion and the comparisons between RCEEP and VI-T/WEC revealed the

negative implications of approximating *D* by VPD. While previous studies discussed this issue (Boese et al., 2017; Lin et al., 2018; Li et al., 2019), RCEEP addresses it by coupling ET and GPP via VI-derived G_c (VI-G_c) rather than VPD. Efforts made by Boese et al. (2017) to improve the performance of uWUE used a different approach, which was found to perform worse than RCEPP (see also Section 3.3), however. As RS VIs were extensively used for characterizing the photosynthetic features of vegetation (Yuan et al., 2010; Yuan et al., 2014; Yan et al., 2015; Zhang et al., 2015), we speculate that the advantages of RCEEP are associated with the ability of RS VIs to characterize biophysical features of terrestrial ecosystems, e.g. canopy structure and greenness, which are important for quantifying photosynthesis of the vegetation canopy, but cannot be successfully estimated in terms of VPD or R_g. Especially when *T* is highly coupled to the atmosphere with a large value of G_c/G_a for the vegetation canopy, where G_a denotes the aerodynamic conductance, *T* is hardly biophysically (i.e., G_c) controlled (Mallick et al., 2016) and thus may be decoupled from photosynthesis. The success of using VIs discloses then the potential of further improving the coupling of biome ET and GPP by considering more biophysical features of ecosystems.

However, the use of VI-G_c may be impeded by the complicated effects of environmental factors in addition to the RS VI. A more complicated formulation of G_c, the effects of multiple environmental factors were accounted for, could be more useful. To clarify this issue, we performed a comparison between the RCEEP version developed in this study and an alternative version that uses a more complex formulation of G_c to account for various environmental effects regarding estimating GPP from ET (Text S1). Interestingly, the result featured comparable performances between the two RCEEP versions (see also Text S1), which revealed no tendencies

of the complex G_c to facilitate a better performance of RCEEP as compared to the VI-G_c. Therefore, the simple formulation of G_c, as indicated by Eq.(6), is sufficient for quantifying GPP using RCEEP along with ET. But this result can only be restricted to the applications of RCEPP. Because the ability of ecosystem ET to indicate environmental controls (Baldocchi and Xu, 2007; Ryu et al., 2008; Ma et al., 2015) on G_c can make up for the shortage of VI-G_c, which explains the success of the application of RCEEP with VI-G_c.

4.3 The potential use of RCEEP and its limitations

RCEEP provides a straightforward approach to understanding the dynamics of GPP in relation to ET. RS-based biophysical process models on coupled estimates of GPP and ET (Chen and Liu, 2020), e.g. the Boreal Ecosystem Productivity Simulator (BEPS) (Chen et al., 2012), Breathing Earth System Simulator (BESS) (Ryu et al., 2011; Jiang and Ryu, 2016), and the coupled diagnostic biophysical model (PML-V2) (Zhang et al., 2019), incorporate process-based modules to simulate GPP and then calculate T in terms of the first or second-order Penman-Monteith equation (Monteith, 1965; Paw U and Gao, 1988) along with GPP-derived g_s (Ball et al., 1987). Such a framework for simulating ET and GPP was also adopted in multiple land surface models (De Kauwe et al., 2013; De Kauwe et al., 2015; Kala et al., 2015). These models can reasonably simulate the variation in ET as a result of GPP but hardly show the responses of GPP to the variations in ET. By contrast, RCEEP proved successful in calculating GPP from ET and can thus provide a reliable and straightforward approach to understanding the responses of GPP to the change of ET. Besides, RCEEP was proved to be more effective than an analogous approach (see also Section 3.3), WEC, which is developed recently (Cheng et al.,

2017). To date, numerous methods have been developed to reasonably reproduce ET on a regional or global scale (Michel et al., 2016; Chen and Liu, 2020; Fisher et al., 2020), therefore, RCEEP can provide an easy approach to estimating regional or global-scale GPP by combing these existing approaches, especially some thermal-driven models which can robustly compute ET based on the energy balance theory in the absence of biome-specific parameters (Long and Singh, 2012; Chen et al., 2013; Mallick et al., 2015; Mallick et al., 2016; Bhattarai et al., 2019).

Our analyses also evidenced that the performances of RCEEP are limited by the ability to characterize the variations in f_T and G_c and could be potentially improved using more appropriate RS factors. First, RCEEP can only be implemented on a daily or larger temporal scale, because the sub-daily variations in G_c are dominated by meteorological factors, which limits the use of VI-G_c on such a time scale. Second, we did not exhaust all the possible RS factors, because this was beyond the scope of this study. Multiple VIs have been explored to represent the biophysical features of vegetation (Wu et al., 2010; Yebra et al., 2013; Zhang et al., 2015; Badgley et al., 2017). All these VIs have the potential of improving RCEEP. For example, leaf chlorophyll concentration (Chl) is known to play an important role in regulating stomatal conductance (Matsumoto et al., 2005), while some RS VIs are capable of characterizing the variations in canopy Chl (Wu et al., 2009). Specific remotely sensed products are tightly correlated with ecosystem photosynthesis. Satellite-retrieved vegetation near-infrared reflectance (NIR_V) (Badgley et al., 2017) and solar-induced chlorophyll fluorescence (SIF) (Mohammed et al., 2019) are further examples of RS retrieved parameters capable of characterizing photosynthesis rate of terrestrial ecosystems for a wide range of biomes (Li et al., 2018; Badgley et al., 2019; Zhang et al., 2020), as they are potentially useful for explaining part of the

photosynthesis dynamics that is independent of transpiration.

5 Conclusion

We developed RCEEP, an RS-driven approach aimed at coupling ecosystem ET and photosynthesis (GPP) on a global scale. RCEEP did not use VPD to approximate *D* in the model as did other generic methodologies but rather estimates ET on the basis of satellite EVI-derived G_c. Besides, to remove the effect of soil evaporation, ET was scaled to *T* using a satellite NDVI-derived f_T. As the newly established approach was developed as an improvement of uWUE model, we compared the performances of RCEEP with uWUE and two additional modified RS-driven versions (VI-T and VI-G), which only incorporate VI-derived f_T (VI-f_T) or G_c (VI-G_c). Relative performances were assessed in terms of the NSE values for reproducing GPP from ET on a daily and monthly scale over 180 flux sites covering 11 biome types over the globe. In addition, considering the recent efforts to partitioning *T* from ET or representing more meaningful relationships between ET and GPP on an ecosystem level, we furtherly compare RCEEP with another three approaches modified from recent studies concerning estimating GPP from ET. The results lead us to the following conclusions:

(a) VI-derived f_T and G_c can help to provide more meaningful relationships between ecosystem ET and GPP, as the three RS-driven approaches, VI-T, VI-G, and RCEEP, exposed more reasonable estimates of GPP compared to the uWUE, which relies on VPD to approximate *D*

(b) RCEEP, incorporating both VI-derived f_T and G_c, yielded the best results and performed better than uWUE over all biome types under investigation on a daily or, with

an exception of EBF, on a monthly scale.

(c) RCEEP featured reliable relationships between ecosystem GPP and ET, with NSE values of 0.73 and 0.78 for reproducing daily and monthly GPP across all sites under investigation.

(d) RCEEP was also found to perform better than another three models, RCEEP-JPL, WEC, and uWUE-Rg, which are modified from recent studies, concerning estimating GPP from ET.

The above results are encouraging in view of a reasonable relationship between ecosystem-level ET and GPP and the coupled modeling of the two fluxes on a global scale, because all RS data used in this study is worldwide available. We did not exhaust all the possible RS factor which are potentially useful for representing plant biophysical features in developing the RCEEP. The model can be further improved in future work, by introducing new RS factors to characterize f_T and G_c and assessing a photosynthesis term that is independent of ET.

Appendix

Appendix A Biome-specific values of the estimated coefficients pertaining to the four approaches presented in Table 1, aimed at coupling ecosystem GPP and ET.

	uWUE	**VI-T**	**VI-G**	**RCEEP**
Biome type	Coefficients [a]			
	w	$w \cdot k_T$	$w \cdot \sqrt{k_G}$	$w \cdot \sqrt{k_G \cdot k_T}$
CRO_C3	3049	5060	3002	3808
CRO_C4	4689	6701	4249	5038
DBF	3820	4594	3078	3367
EBF	3243	4176	3171	3606
ENF/DNF	3165	4683	3435	4136
CSH/OSH	2179	3970	2220	2963
GRA	2698	3999	2717	3314
MF	3827	4838	3193	3562
SAV	3054	5745	2507	3602
WET	2060	3313	2326	2830
WSA	2866	4751	2376	3209
MEAN	3150	4712	2934	3585

[a] Refer to Figure 1 for the definition of each biome type. k_T is dimensionless, and the units of the other two coefficients are k_G: mol m^{-2} s^{-1}; and w: μmol C (mol H_2O)$^{-1}$ $kPa^{0.5}$. But one cannot calculate the value of an individual multiplier using coefficients from different models. For example, we cannot divide the value of $w \cdot k_T$ from VI-T by the w of uWUE, because the averaged effect of $k_T \cdot f_T$ in VI-T has been accounted for by the value of w of uWUE. Values of w, $w \cdot k_T$, $w \cdot \sqrt{k_G}$, and $w \cdot \sqrt{k_G \cdot k_T}$ can only be adopted for the formulations they belong to.

Appendix B NSE values of four models to reproduce GPP from ET over multiple biomes on a daily and monthly scale. MEAN denotes the average across all biome types. Please refer to Figure 1 for the explanation of each biome type.

	Daily				Monthly			
Biome type	uWUE	VI-T	VI-G	RCEEP	uWUE	VI-T	VI-G	RCEEP
CRO_C3	0.45	0.61	0.64	0.70	0.51	0.67	0.62	0.69
CRO_C4	0.65	0.78	0.78	0.83	0.71	0.82	0.76	0.83
DBF	0.56	0.64	0.81	0.83	0.69	0.77	0.85	0.88
EBF	0.15	-0.02	0.42	0.32	0.48	0.27	0.53	0.41
ENF/DNF	-0.02	0.15	0.60	0.65	0.47	0.61	0.68	0.75
CSH/OSH	0.41	0.50	0.70	0.72	0.67	0.73	0.77	0.80
GRA	0.55	0.64	0.73	0.77	0.66	0.75	0.77	0.83
MF	0.43	0.47	0.69	0.69	0.70	0.72	0.78	0.78
SAV	0.57	0.48	0.70	0.71	0.77	0.63	0.77	0.77
WET	0.33	0.48	0.60	0.64	0.40	0.57	0.64	0.69
WSA	0.70	0.62	0.81	0.82	0.85	0.74	0.88	0.89
MEAN	0.43	0.49	0.68	0.70	0.63	0.66	0.73	0.76

Appendix C The analytic water use efficiency (WUE) and inherent water use efficiency (IWUE).

(1) Analytic WUE

Medlyn et al. (2011) proposed a theoretical stomatal conductance model based on the TOSB, assuming that stomatal behavior was optimized for the photosynthesis limited by RuPB generation. The TOSB and the expression of photosynthesis rate as limited by RuPB generation (Arneth et al., 2002) were coupled to derive the 'optimal stomatal control model'.

$$g_s = g_0 + 1.6\left(1+\frac{g_1}{\sqrt{D}}\right)\cdot\frac{A}{C_a}, \quad \text{(C1)}$$

where g_s denotes the stomatal conductance (mol m^{-2} s^{-1}); g_0 the minimum value of g_s; D is the leaf to air vapor pressure difference (kPa); A the net photosynthesis rate (μmol m^{-2} s^{-1}); C_a the CO_2 concentration on the leaf surface (μmol mol^{-1}); and g_1 is a factor controlling the slope of variations in g_s in relation to A. g_1 has an explicit physiological expression, $g_1 \propto \sqrt{\Gamma^*\lambda_m}$, and is a key factor in Eq.(C1)), where Γ^* is the CO_2 compensation point in the absence of dark respiration, and λ_m is the marginal water use efficiency. While assuming g_0 to be 0, integrating Eq. (C1) with the transpiration rate expressed following the Fick's law (Beer et al., 2009; Nobel, 2009):

$$T = g_s \cdot \frac{D}{P_a}, \quad \text{(C2)}$$

where T denotes the transpiration rate (mol m^{-2} s^{-1}), and P_a denotes the atmospheric pressure (kPa); we can derive the following equation (Medlyn et al., 2012), representing the analytic WUE.

$$\mathrm{WUE} = \frac{A}{T} = \frac{C_a \cdot P_a}{1.6\left(D + g_1 \cdot \sqrt{D}\right)}, \quad \text{(C3)}$$

(2) IWUE

IWUE was proposed by Beer et al. (2009) to represent the relationship between ecosystem-level ET and GPP. The value of IWUE is supposed to remain constant for a given biome type under steady-state environmental conditions with a constant value of c_i/c_a. It was defined as follows (Beer et al., 2009):

$$\mathrm{IWUE} = \frac{\mathrm{GPP} \cdot D}{T} = \frac{c_a \cdot (1 - c_i/c_a)}{1.6} \quad , \tag{C4}$$

where T and D are approximated by ET and VPD, respectively.

Appendix D Three approaches bridging ecosystem ET and GPP, modified from recent studies: comparisons with RCEEP.

(1) RCEEP-JPL: RCEEP incorporating f_T derived from the Priestley-Taylor Jet Propulsion Laboratory (PT-JPL)

The ET model Priestley-Taylor Jet Propulsion Laboratory (PT-JPL) (Fisher et al., 2008) is useful for computing f_T and then partitioning T from ET (Gu et al., 2018). PT-JPL is an RS-based ecophysiological ET model, which computes ET as a sum of T, E_i, and E_s, where E_i denotes the canopy interception evaporation. Therefore, f_T can be calculated based on the PT-JPL derived T (T_{JPL}) and ET (ET_{JPL}):

$$f_T = \frac{T_{JPL}}{ET_{JPL}} , \tag{D1}$$

Compared with f_T computed in terms of Eq. (8) along with NDVI in RCEEP, PT-JPL derived f_T (PT-JPL-f_T) explains more physical processes in partitioning T from ET and may have the potential of improving RCEEP. To clarify this issue, we compare the performances between an alternative RCEEP version incorporating PT-JPL-f_T (RCEEP-JPL) and the original version using NDVI-f_T. By substituting $k_T \cdot f_{PAR}$ with PT-JPL-f_T in RCEEP, we derive the alternative version

with PT-JPL-f_T, RCEEP-JPL, such that:

$$\mathrm{GPP} = \left(w \cdot \sqrt{k_G}\right) \cdot \sqrt{\mathrm{sEVI} \cdot \frac{T_{JPL}}{\mathrm{ET}_{JPL}} \mathrm{ET} \cdot P_a^{-1}}\ , \tag{D2}$$

(2) WEC: WUE and ET based carbon uptake model

WEC that estimates GPP using the analytic water use efficiency (WUE) (see also Appendix C-(1)) (Medlyn et al., 2011) and ET was employed by Cheng et al. (2017), to understand the response of the inter-annual dynamics of global carbon uptake in relation to the water cycle. Such that:

$$\mathrm{GPP} = \frac{C_a \cdot P_a}{1.6\left(D + g_1 \cdot \sqrt{D}\right)} \times T\ , \tag{D3}$$

$$T = \mathrm{ET} \cdot f_T = \mathrm{ET} \cdot f_{PAR} \cdot \left(1 - f_{Ei}\right)\ , \tag{D4}$$

where f_{Ei} denotes the proportion of E_i, to ET, and we fix f_{Ei} to 0 for rain-free days. Cheng et al. (2017) computed f_{PAR} in terms of Beer's Law along with RS-derived LAI. In this study, we estimated this variable on the basis of NDVI, according to Eq. (8). *D* in WEC is approximated by VPD. The WEC is analogous to VI-T and also useful for bridging ecosystem ET and GPP, but it adopts the framework of analytic WUE that is different from uWUE.

(3) uWUE-Rg: uWUE incorporating Solar radiation (R_g)

For representing a more meaningful relationship between ecosystem ET and GPP, Boese et al. (2017) modified the uWUE by introducing an additional term, $r \cdot R_g$, where *r* is an empirical factor and R_g denotes the solar radiation, to account for additional ET components, such that:

$$\mathrm{ET} = \frac{\mathrm{GPP}}{\sqrt{D}} + r \cdot R_g\ , \tag{D5}$$

where *D* is approximated by VPD. We could modify this equation to express GPP as a function

of ET:

$$\mathrm{GPP} = \left(\mathrm{ET} - r \cdot R_{\mathrm{g}}\right) \cdot \sqrt{D}\,, \tag{D6}$$

We denoted this method as uWUE-Rg. The term $r \cdot R_{\mathrm{g}}$ is associated with the variations in stomatal conductance, equilibrium evaporation, and the difference between D and VPD and is independent of uWUE term $\mathrm{GPP}/\sqrt{\mathrm{D}}$. This method is suitable to be applied at the site-scale due to the significant spatial variability of the site-specific factor, r, a key parameter for a better coupling of ET and GPP.

Acknowledgments

The authors would like to thank Prof. Torsten Sachs (Helmholtz Centre Potsdam, GFZ German Research Centre for Geosciences) for his valuable comments on this paper. This research is supported by the National Natural Science Fund of China (Grant Nos. 41901342, 31671585), the “Taishan Scholar” Project of Shandong Province, and Key Basic Research Project of Shandong Natural Science Foundation of China (Grant No. ZR2017ZB0422).

Daily flux tower data used for the paper (see also Section 2.4.1 for Table S1) were retrieved from the FLUXNET2015 Tier 2 dataset which is available through https://fluxnet.fluxdata.org/. The site-level MOD09A1 product are available through the Oak Ridge National Laboratory Distributed Active Archive Center (https://modis.ornl.gov/data.html). Detailed information of crop rotations at each crop flux site is available through Bai et al. (2018). This work used eddy covariance data acquired and shared by the FLUXNET community, including these networks: AmeriFlux, AfriFlux, AsiaFlux, CarboAfrica, CarboEuropeIP, CarboItaly, CarboMont, ChinaFlux, Fluxnet-Canada, GreenGrass, ICOS, KoFlux, LBA, NECC, OzFlux-TERN,

TCOS-Siberia, and USCCC. The FLUXNET eddy covariance data processing and harmonization were carried out by the ICOS Ecosystem Thematic Center, AmeriFlux Management Project and Fluxdata project of FLUXNET, with the support of CDIAC, and the OzFlux, ChinaFlux, and AsiaFlux offices.

References

Almeida, J. A. P. (1986), Use of infrared thermometry to measure canopy-air temperature difference at partial cover to assess crop water stress index, The University of Arizona, Tucson, US.

Arneth, A., J. Lloyd, H. Santrùcková, M. I. Bird, S. Grigoryev, Y. N. Kalaschnikov, G. Gleixner, and E. D. Schulze (2002), Response of Central Siberian scots pine to soil water deficit and long-term trends in atmospheric CO2 concentration, *Global Biogeochemical Cycles*, *16*(1), 5.1-5.13.

Badgley, G., C. B. Field, and J. A. Berry (2017), Canopy near-infrared reflectance and terrestrial photosynthesis, *Science advances*, *3*(3), e1602244.

Badgley, G., L. Anderegg, J. Berry, and C. Field (2019), Terrestrial Gross Primary Production: Using NIR V to Scale from Site to Globe, *Global Change Biology*, *25*.

Bai, Y., J. Zhang, S. Zhang, F. Yao, and V. Magliulo (2018), A remote sensing-based two-leaf canopy conductance model: Global optimization and applications in modeling gross primary productivity and evapotranspiration of crops, *Remote Sensing of Environment*, *215*, 411-437.

Bai, Y., J. Zhang, S. Zhang, U. A. Koju, F. Yao, and T. Igbawua (2017), Using precipitation, vertical root distribution, and satellite-retrieved vegetation information to parameterize water stress in a Penman-Monteith approach to evapotranspiration modeling under Mediterranean climate, *Journal of Advances in Modeling Earth Systems*, *9*(1), 168-192.

Baldocchi, D. D., and L. Xu (2007), What limits evaporation from Mediterranean oak woodlands – The supply of moisture in the soil, physiological control by plants or the demand by the atmosphere?, *Advances in Water Resources*, *30*(10), 2113-2122.

Ball, J. T., I. E. Woodrow, and J. A. Berry (1987), A Model Predicting Stomatal Conductance and its Contribution to the Control of Photosynthesis under Different Environmental Conditions, in *Progress in Photosynthesis Research: Volume 4 Proceedings of the VIIth International Congress on Photosynthesis Providence, Rhode Island, USA, August 10–15, 1986*, edited by J. Biggins, pp. 221-224, Springer Netherlands, Dordrecht.

Beer, C., et al. (2009), Temporal and among-site variability of inherent water use efficiency at the ecosystem level, *Global Biogeochemical Cycles*, *23*(2), n/a-n/a.

Bhattarai, N., K. Mallick, J. Stuart, B. D. Vishwakarma, R. Niraula, S. Sen, and M. Jain (2019), An automated multi-model evapotranspiration mapping framework using remotely sensed and reanalysis data, *Remote Sensing of Environment*, *229*, 69-92.

Boese, S., M. Jung, N. Carvalhais, and M. Reichstein (2017), The importance of radiation for semiempirical water-use efficiency models, *Biogeosciences*, *14*, 3015-3026.

Cavanaugh, M. L., S. A. Kurc, and R. L. Scott (2011), Evapotranspiration partitioning in semiarid

shrubland ecosystems: a two-site evaluation of soil moisture control on transpiration, *Ecohydrology*, *4*(5), 671-681.

Chen, J. M., and J. Liu (2020), Evolution of evapotranspiration models using thermal and shortwave remote sensing data, *Remote Sensing of Environment*, *237*, 111594.

Chen, J. M., G. Mo, J. Pisek, J. Liu, F. Deng, M. Ishizawa, and D. Chan (2012), Effects of foliage clumping on the estimation of global terrestrial gross primary productivity, *Global Biogeochemical Cycles*, *26*(1).

Chen, X., Z. Su, Y. Ma, K. Yang, J. Wen, and Y. Zhang (2013), An Improvement of Roughness Height Parameterization of the Surface Energy Balance System (SEBS) over the Tibetan Plateau, *Journal of Applied Meteorology and Climatology*, *52*(3), 607-622.

Cheng, L., L. Zhang, Y.-P. Wang, J. G. Canadell, F. H. S. Chiew, J. Beringer, L. Li, D. G. Miralles, S. Piao, and Y. Zhang (2017), Recent increases in terrestrial carbon uptake at little cost to the water cycle, *Nature Communications*, *8*(1).

Collatz, G. J., J. T. Ball, C. Grivet, and J. A. Berry (1991), Physiological and environmental regulation of stomatal conductance, photosynthesis and transpiration: a model that includes a laminar boundary layer, *Agricultural and Forest Meteorology*, *54*(2), 107-136.

Cowan, I. R., and G. D. Farquhar (1977), Stomatal function in relation to leaf metabolism and environment, *Symposia of the Society for Experimental Biology*, *31*, 471-505.

Croft, H., J. M. Chen, X. Luo, P. Bartlett, B. Chen, and R. M. Staebler (2017), Leaf chlorophyll content as a proxy for leaf photosynthetic capacity, *Global change biology*, *23*(9), 3513-3524.

De Kauwe, M. G., J. Kala, Y. S. Lin, A. J. Pitman, B. E. Medlyn, R. A. Duursma, G. Abramowitz, Y. P. Wang, and D. G. Miralles (2015), A test of an optimal stomatal conductance scheme within the CABLE land surface model, *Geoscientific Model Development*, *8*(2), 431-452.

De Kauwe, M. G., et al. (2013), Forest water use and water use efficiency at elevated CO2 : a model-data intercomparison at two contrasting temperate forest FACE sites, *Glob Chang Biol*, *19*(6), 1759-1779.

Drake, J. E., et al. (2017), Stomatal and non-stomatal limitations of photosynthesis for four tree species under drought: A comparison of model formulations, *Agricultural and Forest Meteorology*, *247*, 454-466.

Fisher, J. B., K. P. Tu, and D. D. Baldocchi (2008), Global estimates of the land–atmosphere water flux based on monthly AVHRR and ISLSCP-II data, validated at 16 FLUXNET sites, *Remote Sensing of Environment*, *112*(3), 901-919.

Fisher, J. B., et al. (2020), ECOSTRESS: NASA's Next Generation Mission to Measure Evapotranspiration From the International Space Station, *Water Resources Research*, *56*(4).

Foken, T. (2008), The energy balance closure problem: an overview, *Ecological Applications*, *18*(6), 1351-1367.

Friedl, M. A. (1995), Modeling land surface fluxes using a sparse canopy model and radiometric surface temperature measurements, *Journal of Geophysical Research: Atmospheres*, *100*(D12), 25435-25446.

Gu, C., J. Ma, G. Zhu, H. Yang, K. Zhang, Y. Wang, and C. Gu (2018), Partitioning evapotranspiration using an optimized satellite-based ET model across biomes, *Agricultural and Forest Meteorology*, *259*, 355-363.

Herrera, A., R. Urich, E. Rengifo, C. Ballestrini, A. González, and W. León (2012), Transpiration in a eucalypt plantation and a savanna in Venezuela, *Trees*, *26*(6), 1759-1769.

738 Idso, S. B. (1982), Non-water-stressed baselines: A key to measuring and interpreting plant water
739 stress, *Agricultural Meteorology*, *27*(1), 59-70.
740 Idso, S. B., R. J. Reginato, and S. M. Farah (1982a), Soil- and atmosphere-induced plant water stress
741 in cotton as inferred from foliage temperatures, *Water Resources Research*, *18*(4), 1143-1148.
742 Idso, S. B., R. J. Reginato, and J. W. Radin (1982b), Leaf diffusion resistance and photosynthesis in
743 cotton as related to a foliage temperature based plant water stress index, *Agricultural*
744 *Meteorology*, *27*(1), 27-34.
745 Jackson, R. D., S. B. Idso, R. J. Reginato, and P. J. Pinter Jr (1981), Canopy temperature as a crop
746 water stress indicator, *Water Resources Research*, *17*(4), 1133-1138.
747 Jasechko, S., Z. D. Sharp, J. J. Gibson, S. J. Birks, Y. Yi, and P. J. Fawcett (2013), Terrestrial water
748 fluxes dominated by transpiration, *Nature*, *496*(7445), 347-350.
749 Jiang, C., and Y. Ryu (2016), Multi-scale evaluation of global gross primary productivity and
750 evapotranspiration products derived from Breathing Earth System Simulator (BESS), *Remote*
751 *Sensing of Environment*, *186*, 528-547.
752 Jin, H., A. Li, J. Bian, X. Nan, W. Zhao, Z. Zhang, and G. Yin (2017), Intercomparison and validation
753 of MODIS and GLASS leaf area index (LAI) products over mountain areas: A case study in
754 southwestern China, *International Journal of Applied Earth Observation and Geoinformation*,
755 *55*, 52-67.
756 Kala, J., M. G. De Kauwe, A. J. Pitman, R. Lorenz, B. E. Medlyn, Y. P. Wang, Y. S. Lin, and G.
757 Abramowitz (2015), Implementation of an optimal stomatal conductance scheme in the
758 Australian Community Climate Earth Systems Simulator (ACCESS1.3b), *Geoscientific Model*
759 *Development*, *8*(12), 3877-3889.
760 Krause, P., D. Boyle, and F. Bäse (2005), Comparison of Different Efficiency Criteria for Hydrologic
761 Models, *Advances in Geosciences*, *5*.
762 Lasslop, G., M. Reichstein, D. Papale, A. D. Richardson, A. Arneth, A. Barr, P. Stoy, and G.
763 Wohlfahrt (2010), Separation of net ecosystem exchange into assimilation and respiration using a
764 light response curve approach: critical issues and global evaluation, *Global Change Biology*,
765 *16*(1), 187-208.
766 Leuning, R. (1995), A critical appraisal of a combined stomatal-photosynthesis model for C3 plants,
767 *Plant, Cell & Environment*, *18*(4), 339-355.
768 Li, X., P. Gentine, C. Lin, S. Zhou, Z. Sun, Y. Zheng, J. Liu, and C. Zheng (2019), A simple and
769 objective method to partition evapotranspiration into transpiration and evaporation at
770 eddy-covariance sites, *Agricultural and Forest Meteorology*, *265*, 171-182.
771 Li, X., et al. (2018), Solar-induced chlorophyll fluorescence is strongly correlated with terrestrial
772 photosynthesis for a wide variety of biomes: First global analysis based on OCO-2 and flux
773 tower observations, *Global Change Biology*, *24*(9), 3990-4008.
774 Lian, X., et al. (2018), Partitioning global land evapotranspiration using CMIP5 models constrained
775 by observations, *Nature Climate Change*, *8*(7), 640-646.
776 Lin, C., P. Gentine, Y. Huang, K. Guan, H. Kimm, and S. Zhou (2018), Diel ecosystem conductance
777 response to vapor pressure deficit is suboptimal and independent of soil moisture, *Agricultural*
778 *and Forest Meteorology*, *250*, 24-34.
779 Lloyd, J., and G. D. Farquhar (1994), 13C discrimination during CO2 assimilation by the terrestrial
780 biosphere, *Oecologia*, *99*, 201-215.
781 Long, D., and V. P. Singh (2012), A Two-source Trapezoid Model for Evapotranspiration (TTME)

from satellite imagery, *Remote Sensing of Environment*, *121*, 370-388.
Ma, N., Y. Zhang, Y. Guo, H. Gao, H. Zhang, and Y. Wang (2015), Environmental and biophysical controls on the evapotranspiration over the highest alpine steppe, *Journal of Hydrology*, *529*, 980-992.
Mallick, K., et al. (2015), Reintroducing radiometric surface temperature into the Penman-Monteith formulation, *Water Resources Research*, *51*(8), 6214-6243.
Mallick, K., et al. (2016), Canopy-scale biophysical controls of transpiration and evaporation in the Amazon Basin, *Hydrol. Earth Syst. Sci.*, *20*(10), 4237-4264.
Matsumoto, K., T. Ohta, and T. Tanaka (2005), Dependence of stomatal conductance on leaf chlorophyll concentration and meteorological variables, *Agricultural and Forest Meteorology*, *132*(1-2), 44-57.
Medlyn, B. E., R. A. Duursma, D. Eamus, D. S. Ellsworth, I. C. Prentice, C. V. M. Barton, K. Y. Crous, P. De Angelis, M. Freeman, and L. Wingate (2011), Reconciling the optimal and empirical approaches to modelling stomatal conductance, *Global Change Biology*, *17*(6), 2134-2144.
Medlyn, B. E., R. A. Duursma, D. Eamus, D. S. Ellsworth, I. Colin Prentice, C. V. M. Barton, K. Y. Crous, P. de Angelis, M. Freeman, and L. Wingate (2012), Reconciling the optimal and empirical approaches to modelling stomatal conductance, *Global Change Biology*, *18*(11), 3476-3476.
Medlyn, B. E., et al. (2017), How do leaf and ecosystem measures of water-use efficiency compare?, *New Phytol*, *216*(3), 758-770.
Michel, D., et al. (2016), The WACMOS-ET project – Part 1: Tower-scale evaluation of four remote-sensing-based evapotranspiration algorithms, *Hydrology and Earth System Sciences*, *20*(2), 803-822.
Mohammed, G., et al. (2019), Remote sensing of solar-induced chlorophyll fluorescence (SIF) in vegetation: 50 years of progress, *Remote Sensing of Environment*, *231*.
Monteith, J. L. (1965), Evaporation and environment, *Symposia of the Society for Experimental Biology*, *19*(19), 205-224.
Mott, K. A., and D. F. Parkhurst (1991), Stomatal responses to humidity in air and helox, *Plant, Cell & Environment*, *14*(5), 509-515.
Nash, J. E., and J. V. Sutcliffe (1970), River flow forecasting through conceptual models part I — A discussion of principles, *Journal of Hydrology*, *10*(3), 282-290.
Nelson, J. A., and B. Bugbee (2015), Analysis of Environmental Effects on Leaf Temperature under Sunlight, High Pressure Sodium and Light Emitting Diodes, *PLoS One*, *10*(10), e0138930.
Nobel, P. S. (2009), Chapter 8 - Leaves and Fluxes, in *Physicochemical and Environmental Plant Physiology (Fourth Edition)*, edited, pp. 364-437, Academic Press, San Diego.
Olufayo, A., C. Baldy, P. Ruelle, and J. Konate (1993), Diurnal course of canopy temperature and leaf water potential of sorghum (Sorghum bicolor L. Moench) under a Mediterranean climate, *Agricultural and Forest Meteorology*, *64*(3), 223-236.
Paw U, K. T., and W. Gao (1988), Applications of solutions to non-linear energy budget equations, *Agricultural and Forest Meteorology*, *43*(2), 121-145.
Perez-Priego, O., G. Katul, M. Reichstein, T. S. El-Madany, B. Ahrens, A. Carrara, T. M. Scanlon, and M. Migliavacca (2018), Partitioning Eddy Covariance Water Flux Components Using Physiological and Micrometeorological Approaches, *Journal of Geophysical Research: Biogeosciences*, *123*(10), 3353-3370.

826 Priestley, C. H. B., and R. J. Taylor (1972), On the Assessment of Surface Heat Flux and Evaporation
827 Using Large-Scale Parameters, *Monthly Weather Review*, *100*(2), 81-92.
828 Reichstein, M., et al. (2005), On the separation of net ecosystem exchange into assimilation and
829 ecosystem respiration: review and improved algorithm, *Global Change Biology*, *11*(9),
830 1424-1439.
831 Ryu, Y., D. D. Baldocchi, S. Ma, and T. Hehn (2008), Interannual variability of evapotranspiration
832 and energy exchange over an annual grassland in California, *Journal of Geophysical Research*,
833 *113*(D9).
834 Ryu, Y., et al. (2011), Integration of MODIS land and atmosphere products with a coupled-process
835 model to estimate gross primary productivity and evapotranspiration from 1 km to global scales,
836 *Global Biogeochemical Cycles*, *25*(4).
837 Sims, D., et al. (2005), Midday values of gross CO2 flux and light use efficiency during satellite
838 overpasses can be used to directly estimate eight-day mean flux, *Agricultural and Forest*
839 *Meteorology*, *131*, 1-12.
840 Stoy, P., et al. (2019), Reviews and syntheses: Turning the challenges of partitioning ecosystem
841 evaporation and transpiration into opportunities, *Biogeosciences*, *16*, 3747-3775.
842 Twine, T. E., W. P. Kustas, J. M. Norman, D. R. Cook, P. R. Houser, T. P. Meyers, J. H. Prueger, P. J.
843 Starks, and M. L. Wesely (2000), Correcting eddy-covariance flux underestimates over a
844 grassland, *Agricultural and Forest Meteorology*, *103*(3), 279-300.
845 Wang, K., R. E. Dickinson, M. Wild, and S. Liang (2010), Evidence for decadal variation in global
846 terrestrial evapotranspiration between 1982 and 2002: 1. Model development, *Journal of*
847 *Geophysical Research*, *115*(D20).
848 Wang, L., S. P. Good, and K. K. Caylor (2014), Global synthesis of vegetation control on
849 evapotranspiration partitioning, *Geophysical Research Letters*, *41*(19), 6753-6757.
850 Wei, Z., K. Yoshimura, L. Wang, D. G. Miralles, S. Jasechko, and X. Lee (2017), Revisiting the
851 contribution of transpiration to global terrestrial evapotranspiration, *Geophysical Research*
852 *Letters*, *44*(6), 2792-2801.
853 Wu, C., Z. Niu, and S. Gao (2010), Gross primary production estimation from MODIS data with
854 vegetation index and photosynthetically active radiation in maize, *Journal of Geophysical*
855 *Research*, *115*(D12).
856 Wu, C., Z. Niu, Q. Tang, W. Huang, B. Rivard, and J. Feng (2009), Remote estimation of gross
857 primary production in wheat using chlorophyll-related vegetation indices, *Agricultural and*
858 *Forest Meteorology*, *149*(6-7), 1015-1021.
859 Yan, H., et al. (2015), Improved global simulations of gross primary product based on a new
860 definition of water stress factor and a separate treatment of C3 and C4 plants, *Ecological*
861 *Modelling*, *297*(0), 42-59.
862 Yang, P., R. Shibasaki, W. Wu, Q. Zhou, Z. Chen, Y. Zha, Y. Shi, and H. Tang (2007), Evaluation of
863 MODIS Land Cover and LAI Products in Cropland of North China Plain Using In Situ
864 Measurements and Landsat TM Images, *IEEE Transactions on Geoscience & Remote Sensing*,
865 *45*(10), 3087-3097.
866 Yebra, M., A. Van Dijk, R. Leuning, A. Huete, and J. P. Guerschman (2013), Evaluation of optical
867 remote sensing to estimate actual evapotranspiration and canopy conductance, *Remote Sensing of*
868 *Environment*, *129*, 250-261.
869 Yuan, W., et al. (2010), Global estimates of evapotranspiration and gross primary production based on

MODIS and global meteorology data, *Remote Sensing of Environment*, *114*(7), 1416-1431.

Yuan, W., et al. (2014), Global comparison of light use efficiency models for simulating terrestrial vegetation gross primary production based on the LaThuile database, *Agricultural and Forest Meteorology*, *192-193*, 108-120.

Zhang, K., J. S. Kimball, Q. Mu, L. A. Jones, S. J. Goetz, and S. W. Running (2009), Satellite based analysis of northern ET trends and associated changes in the regional water balance from 1983 to 2005, *Journal of Hydrology*, *379*(1-2), 92-110.

Zhang, Q., Y.-B. Cheng, A. I. Lyapustin, Y. Wang, X. Zhang, A. Suyker, S. Verma, Y. Shuai, and E. M. Middleton (2015), Estimation of crop gross primary production (GPP): II. Do scaled MODIS vegetation indices improve performance?, *Agricultural and Forest Meteorology*, *200*, 1-8.

Zhang, Y., D. Kong, Q. Zhang, and Y. Yang (2019), Coupled estimation of 500m and 8-day resolution global evapotranspiration and gross primary production in 2002–2017, *Remote Sensing of Environment*, *222*, 165–182.

Zhang, Y., C. Song, G. Sun, L. E. Band, S. McNulty, A. Noormets, Q. Zhang, and Z. Zhang (2016), Development of a coupled carbon and water model for estimating global gross primary productivity and evapotranspiration based on eddy flux and remote sensing data, *Agricultural and Forest Meteorology*, *223*, 116-131.

Zhang, Z., et al. (2020), Reduction of structural impacts and distinction of photosynthetic pathways in a global estimation of GPP from space-borne solar-induced chlorophyll fluorescence, *Remote Sensing of Environment*, *240*.

Zhou, S., B. Yu, Y. Huang, and G. Wang (2014), The effect of vapor pressure deficit on water use efficiency at the subdaily time scale, *Geophysical Research Letters*, *41*(14), 5005-5013.

Zhou, S., B. Yu, Y. Huang, and G. Wang (2015), Daily underlying water use efficiency for AmeriFlux sites, *Journal of Geophysical Research: Biogeosciences*, *120*(5), 887-902.

Zhou, S., B. Yu, Y. Zhang, Y. Huang, and G. Wang (2016), Partitioning evapotranspiration based on the concept of underlying water use efficiency, *Water Resources Research*, *52*(2), 1160-1175.